Sustainable gas conversion by gliding arc plasmas : a new modelling approach for reactor design improvement

Sustainable gas conversion by gliding arc plasmas: a new modelling approach for reactor design improvement.

Senne Van Alphen,*[1,2], Fatme Jardali[1], James Creel[1], Georgi Trenchev[1], Rony Snyders[2] and Annemie Bogaerts[1]

[1] Research group PLASMANT, Department of Chemistry, University of Antwerp, Universiteitsplein 1, 2610 Antwerp, Belgium.

[2] Research group ChIPS, Department of Chemistry, University of Mons, Av. Nicolas Copernic 3, 7000 Mons, Belgium.

Research in plasma reactor designs is developing rapidly as plasma technology is gaining increasing interest for sustainable gas conversion applications, like the conversion of greenhouse gases into value-added chemicals and renewable fuels, and fixation of N_2 from air into precursors of mineral fertilizer. As plasma is generated by electric power and can easily be switched on/off, these applications allows for efficient conversion and energy storage of intermittent renewable electricity. In this paper, we present a new comprehensive modelling approach for the design and development of gliding arc plasma reactors, which reveals the fluid dynamics, the arc behaviour and the plasma chemistry by solving a unique combination of five complementary models. This results in a complete description of the plasma process, which allows one to efficiently evaluate the performance of a reactor and indicate possible design improvements before actually building it. We demonstrate the capabilities of this method for an experimentally validated study of plasma-based NO_x formation in a rotating gliding arc reactor, which is gaining increasing interest as a flexible, electricity-driven alternative for the Haber-Bosch process. The model demonstrates the importance of the vortex flow and the presence of a recirculation zone in the reactor, as well as the formation of hot spots in the plasma near the cathode pin and the anode wall that are responsible for most of the NO_x formation. The model also reveals the underlying plasma chemistry and the vibrational non-equilibrium that exists due to the fast cooling during each arc rotation. Good agreement with experimental measurements on the studied reactor design proves the predictive capabilities of our modelling approach.

Keywords: Reactor design improvement, Gliding arc plasma, Gas conversion, Rotating gliding arc reactor, Plasma-based NO_x production.

1. Introduction

Given the major environmental concerns associated with fossil fuels, a common understanding has been developed that a short-term transition from a carbon-based energy economy to a sustainable one is essential.[1] A key role in this transition will be played by green electricity, as the rapid growth in development and application of photovoltaic cells and wind turbines seem promising for replacing fossil fuels by green electricity on a global scale. However, the intermittent nature of these green energy sources poses challenges in terms of peak shaving and grid stabilisation. The future energy landscape is thus in need of technologies that are inherently flexible to manage the irregular energy supply of green electricity. A technology that harmonizes greatly with the intermittent nature of renewable energy from wind and solar cells is plasma technology.[2,3] Plasma technology delivers the compelling possibility to convert (renewable) electricity into fuels and chemicals, which are much more easily storable energy resources or feedstock for the chemical industry. In these conversion applications, plasma uses electric energy to activate stable, inert gas molecules, like CO_2, CH_4 and N_2, to undergo chemical reactions that would otherwise be thermodynamically unfavoured, creating useful products out of these inert molecules. Plasma technology is inherently flexible, being a so-called "turnkey" process, which can easily be switched on and off, following the energy supply of renewable energy source. Plasma technology of course has to compete with classical (thermal) processes, as well as with other emerging technologies, like electrochemical and photochemical conversion. However, plasma reactors have some advantages, such as low investment and operating costs (scaling linearly with the plant output), and they don't require expensive rare earth metals, which may be a limiting factor for other emerging technologies like electrochemical and photochemical reactors.[2,3] Plasmas are thus a great enabler for a future of sustainable energy, opening the way for the electrification of many industrial applications.[4]

In particular, plasma technology is gaining increasing interest for the conversion of greenhouse gasses (mainly CO_2 and CH_4) into value-added chemicals and liquid fuels, as well as for the conversion of atmospheric N_2 into NH_3 and NO_x for mineral fertilizers.[2–5] The applied electric power selectively heats the electrons in the plasma, which collide with the gas molecules, causing excitation, ionization and dissociation of these molecules. The excited species, ions and radicals quickly react further, creating new molecules. As energy is predominantly transferred to the electrons (typically reaching energies of a few eV, i.e., several 10 000 K), the bulk gas (virtually at room temperature up to a maximum of a few 1000 K) does not have to be heated as a whole for the conversion process, unlike in classical thermal conversion. It is the selective energy transfer to electrons, creating a thermal non-equilibrium between electrons and gas molecules, that gives plasma reactors an edge over thermal reactors regarding the energy effiency.[4]

These sustainable chemistry processes have already been tested in different kind of plasma reactors, the most prevalent being microwave (MW)[6–10], gliding arc (GA)[11–16], and dielectric barrier discharge (DBD) plasmas.[17–21] GA plasma reactors have especially piqued the interest of industry, as they deliver energy-efficient conversion, operate at atmospheric pressure and are well suited for industrial applications and upscaling, given their simplicity and reliability.[4] In its simplest geometry, a GA reactor is built by applying a gas flow and a high voltage between two blade-shaped electrodes. The arc self-initiates at the narrowest gap, where gas enters the reactor, then travels through the reactor forced by the gas flow. When the distance between the electrodes becomes too large for the arc to sustain, it extinguishes and a new arc is initiated at the narrowest gap. This classical GA geometry has been investigated for several sustainable chemistry applications during the past decade, demonstrating the potential of GA reactors for sustainable and efficient gas conversion.[12,13,22] Indeed, this research showed that electrons in GA discharges mainly vibrationally excite gas molecules, like N_2 and CO_2, which is a very efficient activation mechanism for further dissociation of these molecules.[22] However, this basic reactor design suffers from a couple of problems. The flat two-dimensional (2D) electrode geometry leads to extremely non-uniform gas treatment, as a significant amount of gas does not flow

through the arc, or even flows around it as it glides upwards.[23,24] Furthermore, the reactor deteriorates fast due to strong electrode degradation, as a result of the high current density of the discharge.

For this reason, novel GA designs have been developed, aiming to improve the electrode lifetime, ionization efficiency and gas conversion. These new envisaged reactor designs abandon the classical 2D configuration and opt for a three-dimensional (3D) cylindrical geometry that introduces the gas stream through tangentially oriented gas inlets. This initiates a vortex swirl flow along the walls of the reactor, partially isolating the plasma from the reactor walls, hence increasing electrode (reactor) lifetime, and capturing the arc in a so-called 'tornado flow'. A great number of experiments, as well as some numerical simulations, have been conducted to evaluate these kind of new 3D GA designs for sustainable chemistry applications, like N_2 fixation, CO_2 conversion and dry reforming of CH_4, demonstrating promising results compared to other plasma reactor types. [14–16,25–27] Furthermore these 3D designs provide the possibility to combine them with a catalyst bed, to improve the selectivity of the plasma-based process towards desired end-products.[28–30]

While the above papers demonstrate the potential of GA reactors, further optimisation is definitely needed to make the process industrially relevant. The optimal operation conditions and plasma parameters for maximal conversion and energy efficiency still remain unknown for many of these reactors. Furthermore, the reactor design leaves considerable room for improvement. Even in these 3D designs, a significant amount of gas passes around the plasma without being converted.[14,27]

In this paper, we present a unique modelling approach, that can be used for modelling-based reactor design development and reactor design improvement. Computational models allow one to simulate the performance of a reactor design, delivering valuable insight in possible design improvements and optimal operating conditions, before actually building a prototype, saving a lot of time and money in the optimisation process. Given the transient nature of a GA and the complex plasma chemistry occurring between electrons, ions, radicals, and excited species, modelling GA reactor designs is a very challenging task.[31–35] Describing the fluid dynamics of the gas flow, as well as the electrical properties

of the arc, together with the plasma chemistry in a 3D geometry, would require a prohibitively long computation time. Therefore, our new modelling approach circumvents this problem, by solving each aspect of the reactor, i.e. the fluid dynamics, the arc behaviour and the plasma chemistry, individually in separate models. These models are solved in a complementary manner, in which the result of one model serves as input for the next, eventually describing the entire plasma reactor behaviour. While this approach allows for a comprehensive description of any GA plasma-based gas conversion application, we present the methodology of the approach for N_2 fixation into NO_x (i.e. NO and NO_2) in a rotating gliding arc (RGA) reactor. This process is gaining increasing interest as a flexible, electricity-driven alternative for the Haber-Bosch process.[5,36] The plasma-based process requires air as its only resource, which eliminates the energy-intensive H_2 production needed for the classical Haber-Bosch process, giving it an edge over the classical process when it is optimized towards its limit."

2. Model description

The modelling strategy we developed considers all aspects needed to reveal the underlying mechanisms in the RGA design, by five complementary models: a 3D turbulent gas flow model, a 3D thermal plasma model, a 2D non-thermal plasma model, 3D particle tracing simulations and a quasi-1D plasma chemistry model. Decoupling these five models allows us to tailor our assumptions specifically to each model, which drastically decreases the complexity and calculation time of each model. For instance, we can assume a simplified chemistry set in the calculation of our physical parameters, speeding up these computationally heavy 3D simulations, since we simulate the chemistry in more detail in our quasi-1D simulation. Hybrid models, which combine different modelling approaches for different species or processes, to take benefit of their strengths and avoid their limitations, do exist in plasma research for many years, but to our knowledge, such a hybrid modelling approach that we propose here does not yet exist in literature. These models are solved sequentially in which each model builds further on the results of the previous calculations. We describe here the computational details of each model in the sequence they are solved.

2.1 Reactor geometry

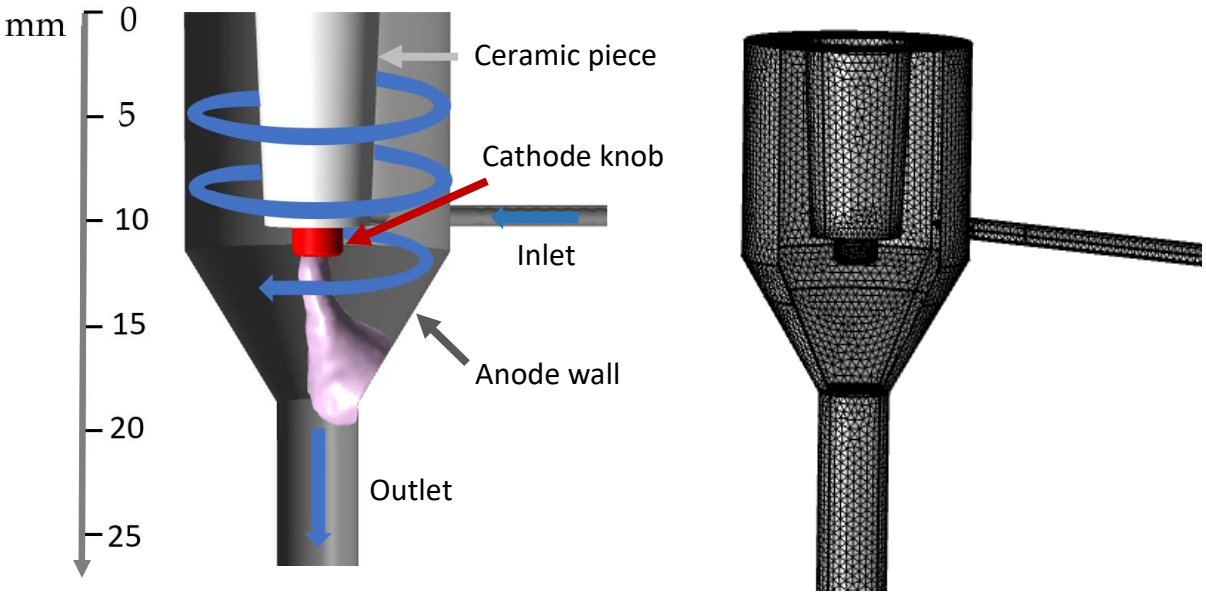

Figure 1: The RGA reactor geometry and its finite element mesh in the model.

The geometry of the RGA reactor is shown in figure 1, along with its finite element mesh used in the 3D model. The reactor body is a cylinder with radius of 6.5 mm and height of 11.2 mm, connected to a cone that narrows the reactor tube down to 2 mm in radius at the outlet. The gas enters the reactor tangentially through an inlet tube with radius of 0.5 mm and length of 25 mm, at a typical flow rate of 2 L min^{-1}. The cathode pin in the centre of the reactor is enclosed by a piece of ceramic (100 mm in length, 3 mm in radius) so only a cylindrical knob with 1.3 mm radius and 1.4 mm length is exposed. The arc is formed between this cathode knob (i.e., high-voltage electrode, with typical applied voltage around 2-3 kV), and the anode reactor wall, which remains at ground potential.

2.2 3D Turbulent flow model

In our models we consider an N_2-O_2 gas mixture, for which the gas properties are added to the Electronic Supporting Information (ESI; section S1). We describe the behaviour of the gas flow in the reactor using computational fluid dynamics (CFD). Given the high internal flow speed (53 m/s at the inlet, for a flow rate of 2 L min^{-1}) and the somewhat complex reactor geometry, a high level of turbulence is expected in the flow, which makes solving the classical Navier-Stokes equations in their

full form computationally very intensive. For this reason, we simulate the gas flow using a Reynolds-averaged-Navier-Stokes (RANS) turbulent model, which significantly reduces the computation time by averaging all fluctuating turbulent quantities over time. In general, all RANS models solve the following mass continuity and momentum continuity Navier-Stokes equations for a Newtonian fluid:

$$\nabla.\left(\rho\overrightarrow{u_g}\right) = 0 \tag{1}$$

$$\rho\left(\overrightarrow{u_g}.\nabla\right)\overrightarrow{u_g} = \nabla.\left[-p\vec{I} + (\mu+\mu_T)\left(\nabla\overrightarrow{u_g} + \nabla\left(\overrightarrow{u_g}\right)^T\right) - \frac{2}{3}(\mu+\mu_T)\left(\nabla.\overrightarrow{u_g}\right)\vec{I} - \frac{2}{3}\rho k_T\vec{I}\right] + \vec{F} \tag{2}$$

Where ρ stands for the gas density, $\overrightarrow{u_g}$ is the gas flow velocity vector, superscript T stands for transposition, p is the gas pressure, μ is the dynamic viscosity and μ_T the turbulent viscosity of the fluid, k_T is the turbulent kinetic energy, $\vec{I}$ is the unity tensor and $\vec{F}$ is the body force vector. The turbulent flow model is solved independently from the other four models, i.e., we assume that the flow in the reactor is not influenced by the heat produced by the plasma or by changes in gas composition due to chemical reactions. This assumption is valid as any influences from gas heating are small in comparison to the strong background inflow from the inlet, while the chemical conversion is too limited (i.e. % range) to significantly change the physical properties of the flow.

We use the Menter's Shear Stress Transport (SST) model,[37] which uses the common k-ε model in the free stream and combines it with the more accurate k-ω model near the walls, where the flow is more complicated. More information about the SST model is given in the ESI (section S2). The model is solved using the CFD module of COMSOL version 5.5.[38]

2.3 3D Thermal plasma model

To simulate the plasma arc behaviour in 3D, we modelled the reactor geometry in figure 1 as part of an electric circuit: a 3 kV voltage source was connected to the cathode, while the walls were kept grounded. The electric circuit also includes a ballast resistor and a capacitor, as explained in more detail in the ESI (section S3). The gas breakdown and the arc formation between cathode pin and anode wall

is simulated by solving a current conservation equation based on Ohm's law, using the electric potential (V) and the electric conductivity (σ) as dependent variables.

$$\nabla \cdot \vec{J} = 0 \tag{3}$$

$$\vec{J} = \sigma \vec{E} \tag{4}$$

$$\vec{E} = -\nabla V \tag{5}$$

Here $\vec{J}$ is the current density and $\vec{E}$ is the electric field. Additionally, this model calculates the rise in gas temperature and the corresponding rise in electric conductivity, as electric current flows through the gas between cathode and anode. The temperature dependency of the electric conductivity is given by an interpolation table in the ESI (section S1) The gas temperature is calculated by the gas thermal balance equation.

$$\rho C_p \frac{\partial T_g}{\partial t} + \rho C_p \overrightarrow{u_g} \cdot \nabla T_g - \nabla \cdot \left(k_g \nabla T_g\right) = Q \tag{6}$$

Where ρ is the gas density, C_p is the gas heat capacity at constant pressure, k_g is the gas thermal conductivity, T_g is the gas temperature and Q is a heat source term, which includes Ohmic heating (due to the electric current) and radiation loss.

As this heat transfer equation is coupled to the results of the turbulent flow model through $\overrightarrow{u_g}$, the thermal plasma model takes into account the behaviour of the gas flow when calculating the movement of the arc. This is needed to simulate the so-called "gliding" behaviour of a GA, in which the gas drags the arc along the flow.

2.4 2D Non-thermal plasma model

While the thermal plasma model can correctly describe the gas temperature gradients and 3D movement of the arc, it overestimates the absolute value of the gas temperature. Indeed, the model assumes that the plasma is in thermal equilibrium, meaning that the gas temperature and electron temperature are equal at any point in the discharge. GA plasmas, however, are known to be "quasi-

thermal" or "warm" plasmas, that induce a thermal non-equilibrium by selectively providing the electric energy to the electrons.[14,16,22,27] As a result, the gas temperature calculated by the thermal model is too high and needs to be corrected (details about the correction are given in ESI section S4). This correction is provided by a more comprehensive non-thermal plasma model that explicitly describes the behaviour of the various plasma species, i.e., the electrons, various ions, radicals, excited species and molecules. To avoid prohibitively long calculation times, however, we assume a quasi-neutral plasma, in which the electron and total ion densities are equal at all times. This is achieved by calculating the density of one ion ($n_{NO_2^-}$) by balancing the electron density (n_e) with the densities of the other ions ($n_{N_2^+}, n_{O_2^+}, n_{NO^+}$) :

$$n_{NO_2^-} = \left(n_{N_2^+} + n_{O_2^+} + n_{NO^+} - n_e\right) \tag{7}$$

This approach has a drawback that it cannot resolve the formation of Debye sheaths at the cathode and anode of the reactor. The latter description would however require a finite element mesh in the order of micrometers to be solved correctly, while the sheaths do not have significant influence on the final solution for the arc column.

The model solves the following equation for the various neutral species, balancing the diffusion and convection of each plasma species with its production and loss rates due to chemical reactions:

$$\frac{\partial n}{\partial t} + \nabla(D\nabla n) + (\overrightarrow{u_g}.\nabla)n = R \tag{8}$$

In which n is the species density, D is the diffusion coefficient, $\overrightarrow{u_g}$ the gas flow velocity vector and R the sum of all production and loss rates due to chemical reactions.

For the ions, an extra ion mobility (μ_i) term is added to the above equation, to account for their migration due to the ambipolar electric field ($\overrightarrow{E_{amb}}$):

$$\frac{\partial n_i}{\partial t} + \nabla\left(D_i\nabla n_i + \mu_i n_i \overrightarrow{E_{amb}}\right) + (\overrightarrow{u_g}.\nabla)n_i = R \tag{9}$$

For the electrons, the migration is calculated in the same way, using the electron mobility (μ_e):

$$\frac{\partial n_e}{\partial t} + \nabla\left(D_e \nabla n_e - \mu_e n_e \overrightarrow{E_{amb}}\right) + (\overrightarrow{u_g}.\nabla) n_e = R \tag{10}$$

The average electron energy $\bar{\varepsilon}_e$ is calculated through:

$$\frac{\partial n_e \bar{\varepsilon}_e}{\partial t} + \nabla.\left(-\mu_{\varepsilon,e} n_e \overrightarrow{E_{amb}} - D_{\varepsilon,e} \nabla(n_e \bar{\varepsilon}_e)\right) + \left(\overrightarrow{u_g}.\nabla\right) n_e \bar{\varepsilon}_e = q_e \vec{E}.\overrightarrow{G_e} + n_e \Delta\bar{\varepsilon}_e + Q_{bg} \tag{11}$$

Where n_e is the electron density, q_e the elementary charge, $\vec{E}$ the externally applied electric field, $\Delta\bar{\varepsilon}_e$the energy exchanged in inelastic collisions with molecules, and Q_{bg} the background heat source serving as a stabilization term for the simulation. The terms $\mu_{\varepsilon,e}$ and $D_{\varepsilon,e}$ stand for the electron energy mobility and diffusion coefficient, respectively:

$$\mu_{\varepsilon,e} = \frac{5}{3}\mu_e \tag{12}$$

$$D_{\varepsilon,e} = \frac{2}{3}\mu_{\varepsilon,e}\bar{\varepsilon}_e \tag{13}$$

With μ_e the electron mobility. The electron flux $\overrightarrow{G_e}$is derived from:

$$G_e = -D_e \nabla n_e - \mu_e n_e \overrightarrow{E_{amb}} \tag{14}$$

With D_e the electron diffusion coefficient. The ambipolar electric field $\overrightarrow{E_{amb}}$ is solved as follows:

$$\overrightarrow{E_{amb}} = \frac{\nabla n_i(-D_e + D_i)}{n_i(\mu_i + \mu_e)} \tag{15}$$

Finally, instead of the Poisson equation, the charge conservation equation is solved using following Laplace equation:

$$\nabla\left[\sigma_{pl}(-\nabla\varphi)\right] = 0 \tag{16}$$

Where σ_{pl} stands for the plasma conductivity and φ stands for the electric potential.

$$\sigma_{pl} = |q_e|(\mu_e n_e + \mu_i n_i) \tag{17}$$

Solving this non-thermal plasma model in 3D, including the transport and reactions of all species in an N_2/O_2 plasma, would require an excessively long computation time. Therefore, the model is calculated for a 2D axisymmetric geometry with a limited chemical reaction set, as described in section 2.7 below. This approach was already evaluated by Trenchev et al. for CO_2 conversion in other types of plasma reactors with very satisfying results.[32,39,40] As this model correctly incorporates the heat terms of all plasma processes and reactions occurring in an N_2/O_2 plasma, the results from this 2D model can be used to correct the gas temperature of the 3D thermal model, as explained in the ESI (section S4). We assume that the temperature calculated in a 2D axisymmetric non-thermal plasma model can be used as a reference to assess the temperature in an arc moving in three dimensions. This assumption is based on the fact that the magnitude of the main heat source, i.e. the exothermic plasma reactions, remains the same in an axial symmetric reactor geometry.

2.5 Quasi-1D plasma chemistry simulations

To reveal the chemical pathways of NO_x formation and to calculate the NO_x yield in this GA plasma reactor, we apply a quasi-1D chemical kinetics model, using the zero-dimensional plasma kinetics solver, ZDPlasKin.[41] This model provides the time evolution of the number density of all chemical species by solving the following continuity equation for the various species, taking into account the production and loss terms by the chemical reactions:

$$\frac{dn_i}{dt} = \sum_j \left[\left(a_{ij}^R - a_{ij}^L\right) k_j \prod_l n_l^L \right] \tag{18}$$

In which n_i is the density of species i and a_{ij}^R and a_{ij}^L are the stoichiometric coefficients of species i on the right-hand and left-hand side of the reaction j, respectively. n_l is the density of the reacting species l. k_j is the reaction rate coefficient of reaction j, which has the general form:

$$a_A\, A + \, a_B B \, (+\Delta H) \xrightarrow{k_j} a_c C + \, a_D D \, (+\Delta H) \tag{19}$$

In which A, B, C and D are the species, and a_A , a_B, a_c and a_D their stoichiometric coefficients. ΔH represents the reaction enthalpy. The rate coefficients of the heavy particle reactions are taken from literature and are a function of the gas or electron temperature, whereas the rate coefficients for the electron impact reactions are calculated using the electron impact cross sections and the electron energy distribution function through the BOLSIG+ Boltzmann solver built into ZDPlasKin.[42] This Boltzmann routine solves the Boltzmann equation for the electrons using a two-term approximation to calculate the electron energy distribution function.

In this model, transport processes are not considered, i.e., the species densities are assumed to be constant in the entire simulation volume, allowing for the incorporation of an extensive plasma chemistry set without suffering from long calculation times. Hence, this modelling approach is commonly called a 0D or global model.[43] However, by means of the gas velocity the time evolution of the simulation can be translated to a spatial variation (i.e., following the path of the gas molecules), so this model behaves as a "quasi-1D" model. In order to account for the spatial variations, the output from the above 3D models (i.e., the gas temperature and power density profiles) is used as input for this quasi-1D model, from the particle tracing simulations, as described in the next section.

2.6 Particle tracing simulations

The particle tracing simulations serve as the bridge between the 3D models and the quasi-1D chemical kinetics model, as they are able to convert the calculated plasma parameters of the 3D models to a time-based input for the quasi-1D model. These simulations compute the trajectory of gas molecules through the reactor and report the "conditions" (i.e., gas temperature and power density) the molecules experience as a function of time, as they flow through the plasma towards the outlet. These trajectories are calculated based on the drag force imposed by the velocity fields that were previously computed by the 3D models.

$$\frac{d(m_p v)}{dt} = F \tag{20}$$

More information about the calculation of the drag force is given in ESI (section S5). This force only takes into account the convection of the molecules due to the turbulent gas flow, while neglecting any transport through diffusion (and migration for charged particles). Due to the high velocity in the vortex flow of the reactor, convection is the most significant mode of transport for all chemical species, justifying this assumption. We performed the trajectory calculations for 10,000 particles, i.e., gas molecules, to ensure statistically relevant results. This yields 10,000 possible trajectories which the gas molecules can follow when flowing through the reactor, as well as the corresponding gas temperature and power density they experience along their trajectories. In principle, these 10,000 trajectories could serve as input for 10,000 different quasi-1D calculations, each calculating the NO_x concentration for a fraction of 1/10,000 of the gas, as it follows one of the calculated trajectories throughout the reactor. However, many of the gas molecules experience similar conditions, so we group trajectories that experience a similar maximum temperature in the plasma and we compute the average values. By applying this averaging method, we narrow the 10,000 trajectories down to ten average trajectories, each describing the specific plasma conditions (i.e., gas temperature and power density) that the gas experiences as it follows that trajectory. These gas temperature and power density profiles are used in the above quasi-1D chemical kinetics simulation, for each of the ten trajectories, calculating the underlying chemistry, and the NO_x concentration that is achieved in each group. Finally, the overall NO_x concentration is calculated from a weighted average of the ten simulations, determined by the number of particles in each group.

2.7 Plasma chemistry included in the models

The full chemistry set used in the quasi-1D chemical kinetics model was recently developed and validated for another type of GA plasma (GA plasmatron) by Vervloessem et al.[27] The reactions and corresponding rate coefficients, and the references where these data were adopted from, are listed in the ESI (section S6). The chemistry set includes 82 different species, which are presented in table 1. The reduced chemistry set of the 2D non-thermal plasma model contains 21 species, which are

highlighted in blue bold face in table 1. In addition, in this reduced set the vibrational levels of N_2 and O_2 are considered as 1 lumped level, which is further explained in the ESI (section S7). The total set incorporates 1,214 electron impact reactions, 481 ionic reactions and 432 neutral reactions, as well as 2,478 vibration-vibration exchanges and vibration-translation relaxations between molecular and atomic nitrogen and oxygen, as detailed in the ESI (section S6). Plasma-wall interactions do not occur in our RGA reactor, because the vortex swirl flow isolates the plasma from the wall to improve electrode lifetime. The reduced chemistry set includes 664 electron impact reactions, 25 ionic reactions and 124 neutral reactions, as well as 2,478 vibration-vibration exchanges and vibration-translation relaxations between molecular and atomic nitrogen and oxygen; these reactions are also highlighted in blue bold face in the ESI (section S6).

Table 1. Different plasma species included in the model. The symbol "V" followed by a number stands for the vibrational level of that species. Species included in the reduced chemistry set of the 2D model are presented in blue bold face.

Neutral species	Radicals	Charged species	Excited species
$\mathbf{N_2}$, $\mathbf{O_2}$, $\mathbf{O_3}$,	**N**, N(2D), N(2P),	$\mathbf{e^-}$ N^+, $\mathbf{N_2^+}$, N_3^+, N_4^+,	$\mathbf{N_2(V1-V24)}$, $\mathbf{O_2(V1-V15)}$,
$\mathbf{NO}$, $\mathbf{NO_2}$, N_2O,	**O**, O(1D), O(1S)	O^-, O_2^-, O_3^-, O_4^-,	$\mathbf{N_2(A^3\Sigma_u^+)}$, $\mathbf{N_2(B^3\Pi_g)}$, $\mathbf{N_2(C^3\Pi_u)}$, $\mathbf{N_2(a'^1\Sigma_u^-)}$, $\mathbf{O_2(a^1\Delta)}$, $\mathbf{O_2(b^1\Sigma^+)}$,
NO_3, N_2O_3,		O^+, $\mathbf{O_2^+}$, O_4^+,	$\mathbf{O_2(A^3\Sigma^+, C^3\Delta, c^1\Sigma^-)}$*
N_2O_4, N_2O_5		$\mathbf{NO^+}$, NO_2^+, N_2O^+, NO^-, $\mathbf{NO_2^-}$, N_2O^-, NO_3^-, $O_2^+N_2$	

* $O_2(A^3\Sigma^+, C^3\Delta, c^1\Sigma^-)$ is a combination of three states with a threshold energy of 4.5 eV.

3. Results and discussion

To display the capabilities of our model to fully describe the performance of a GA reactor design, we present all the aspects of the flow and plasma behaviour in our RGA reactor in five sections. First we describe the 3D gas flow patterns, the arc formation, and the 3D arc rotation in this design. Then we discuss the gas molecules trajectories, as they flow through the plasma. Next we evaluate the performance of the reactor design by calculating the overall NO_x concentration. Subsequently we reveal the underlying plasma chemistry. Finally, we illustrate the predictive capability of the model by comparing the modelling results to experimental measurements in the RGA reactor.

a. 3D gas flow pattern and arc behaviour

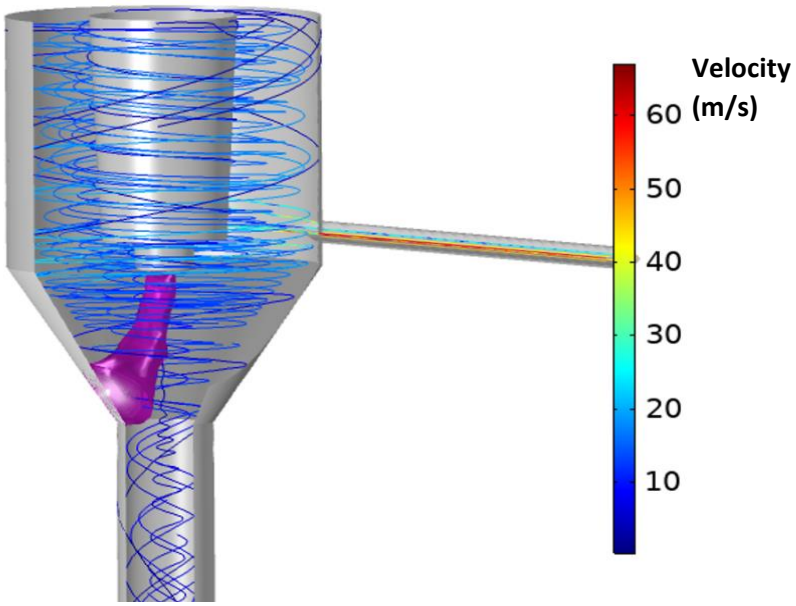

Figure 2: Calculated gas velocity streamlines and arc formation in the RGA reactor.

The RGA reactor under study is characterised by its rotational gas flow, designed specifically to create rotational movement of the arc as it is dragged along the rotating gas stream (hence the name of the reactor). As shown by the gas velocity stream lines in figure 2, calculated by the 3D turbulent flow model, this flow pattern is initiated by the high velocity stream of ~60 m/s in the tangential gas inlet. As the gas is released from the inlet tube and enters the reactor body, it follows the vortex flow pattern along the reactor walls, with a typical velocity up to ~30 m/s. As the gas spirals along the reactor walls towards the outlet, it loses its momentum, eventually slowing down to a typical velocity of 10 m/s when it leaves the reactor.

Figure 3 presents the values of the flow velocity in a horizontal and vertical cross section of the reactor, showing a significant difference in flow velocity near the walls (i.e. ~20-30 m/s) and in the centre of the reactor (i.e. 2 m/s). The vortex flow in the reactor is thus characterized by a high-velocity peripheral stream along the reactor walls and a much slower flow near the centre.

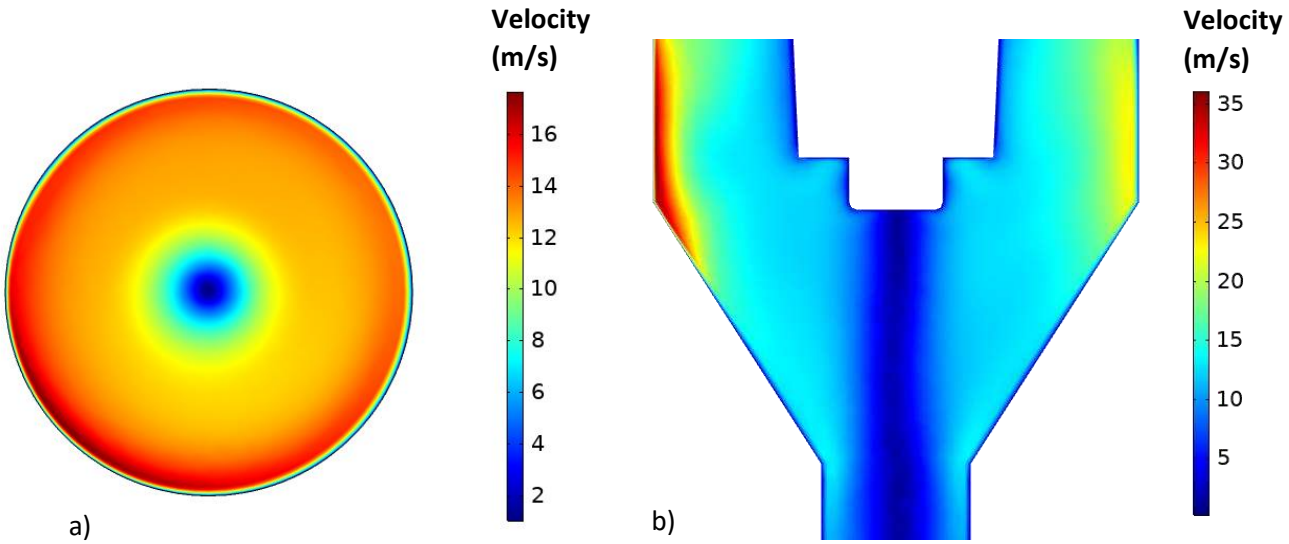

Figure 3: Gas velocity magnitude in the (a) horizontal cross section (1 mm under the cathode) and (b) vertical cross section (reactor center) of the RGA reactor.

The arc ignites in the shortest gap between the cathode pin and the anode wall and follows the rotational movement of the gas. Figure 2 only presents a snapshot of the arc (at 1.6 ms), but when looking at the temporal behaviour, one end of the arc remains attached to the cathode pin while the other glides over the reactor walls (anode), as it is dragged around by the gas flow.

This rotation is illustrated by the sequence of calculated power density profiles in figure 4, as obtained from the 3D thermal arc model. These profiles demonstrate where the power is applied to the gas and thus where the plasma is formed. In these profiles, most of the power is applied near the cathode pin and anode wall (red power density hotspots), which is where most electrons and reactive plasma species will thus be created. The sequence of power profiles also clearly shows the rotation period of the arc, as ~1.75 ms.

As the arc rotates, it quickly heats the gas. This rise in gas temperature is calculated by the 3D thermal plasma model based on Joule heating, to which the correction of the 2D non-thermal plasma model adds the effect of the exothermic plasma chemistry. The reactions contributing most to this effect are the conversion of NO into NO_2 and the relaxation of vibrationally excited molecules. The gas heating is illustrated by the sequence of calculated temperature profiles in figure 5, as obtained from the 3D thermal arc model (again corrected by means of the 2D non-thermal arc model). Like the rotation of the power density, we observe the rotation of a very hot plasma zone, reaching temperatures up to 3500 K. These peak temperatures are found in the same locations as the power density hotspots, because gas heating is here the most pronounced, but the high temperatures are also spread out to some extent, due to thermal conductivity. The rotation of this very hot plasma zone initiates significant temperature swings: at a fixed position in the reactor, the temperature can change from 3500 K to room temperature every 1.75 ms.

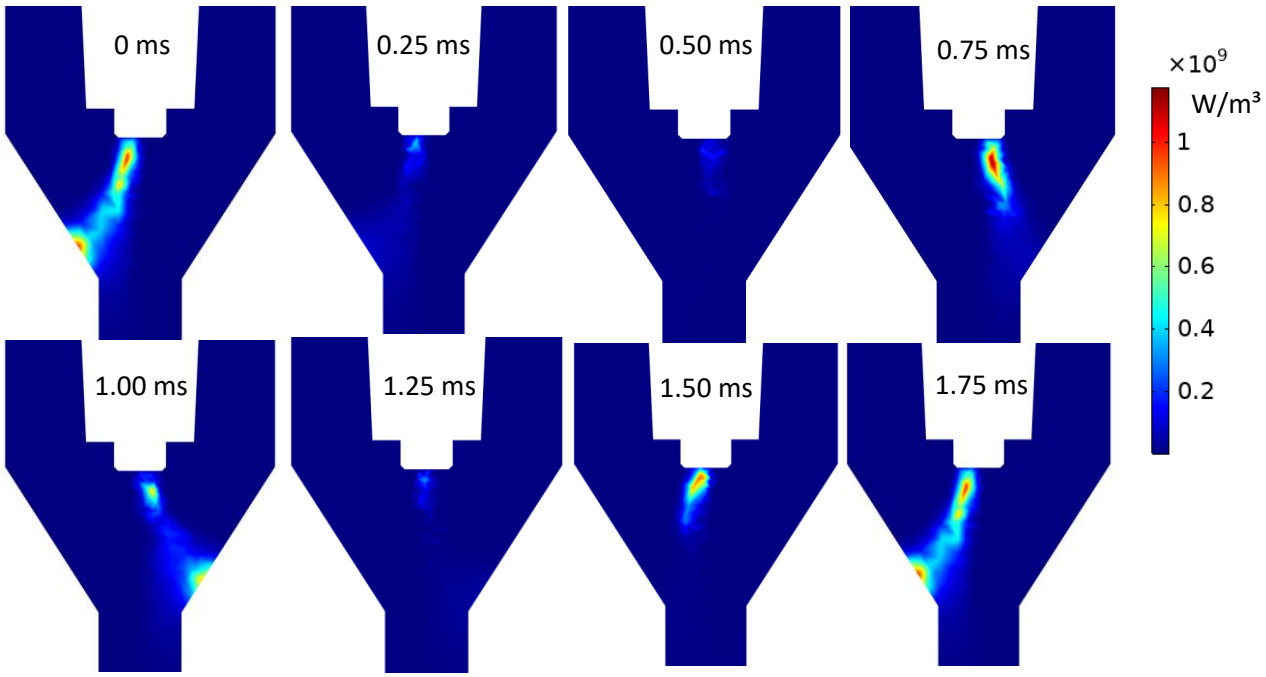

Figure 4: Calculated power density profiles at different time instants during the rotation of the plasma arc.

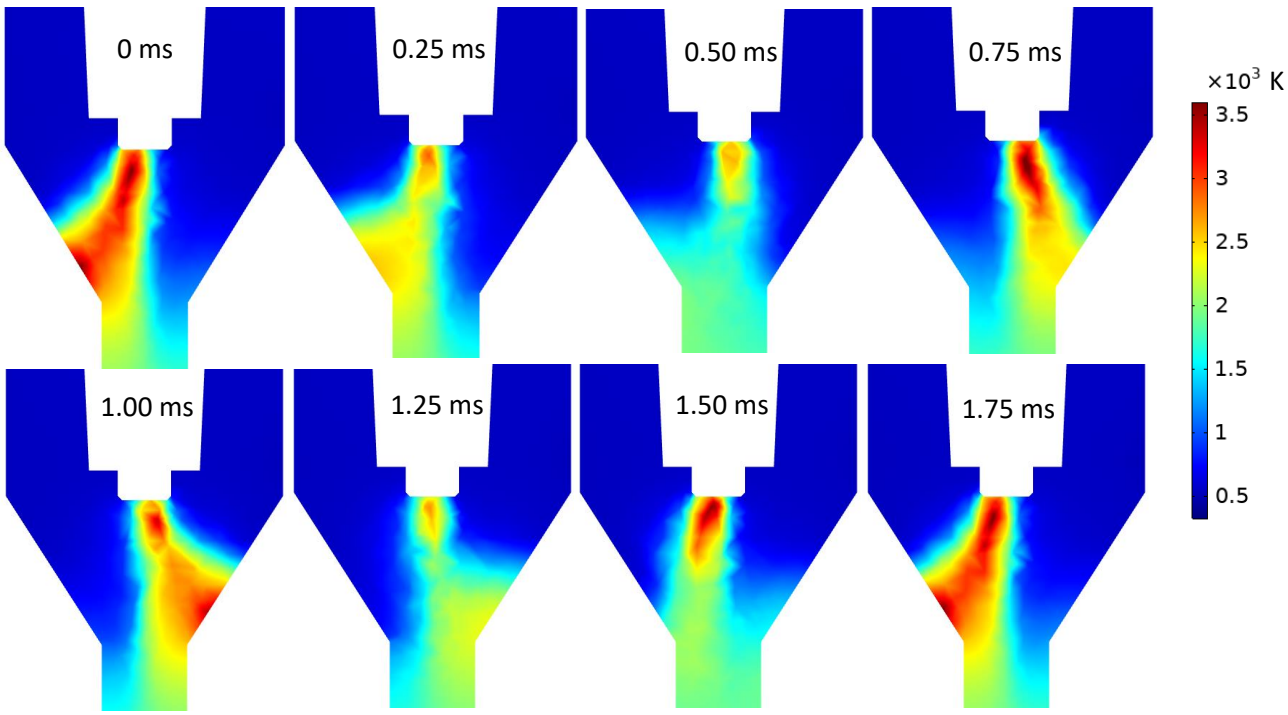

Figure 5: Calculated plasma gas temperature profiles at different time instants during the rotation of the plasma arc.

As the hot plasma arc is responsible for the creation of plasma species that enable the plasma-based NO_x production, the achieved NO_x concentration in the RGA depends greatly on the fraction of the gas that flows through these rotating hot zones and the residence time within them. This is explained in detail in the next section.

3.2 Gas molecule trajectories

The particle tracing simulations reveal the residence time which the gas molecules experience while flowing in between the electrodes of the reactor. This is illustrated by the histogram in figure 6, showing the wide distribution of residence times that the gas molecules experience when flowing between the electrodes of the reactor, ranging from less than 1.75 ms up to even 17.5 ms. The majority of the gas molecules (i.e. 79 % of the gas), however, is either less than 1.75 ms or between 3.5 ms and 5.25 ms in the active zone of the reactor.

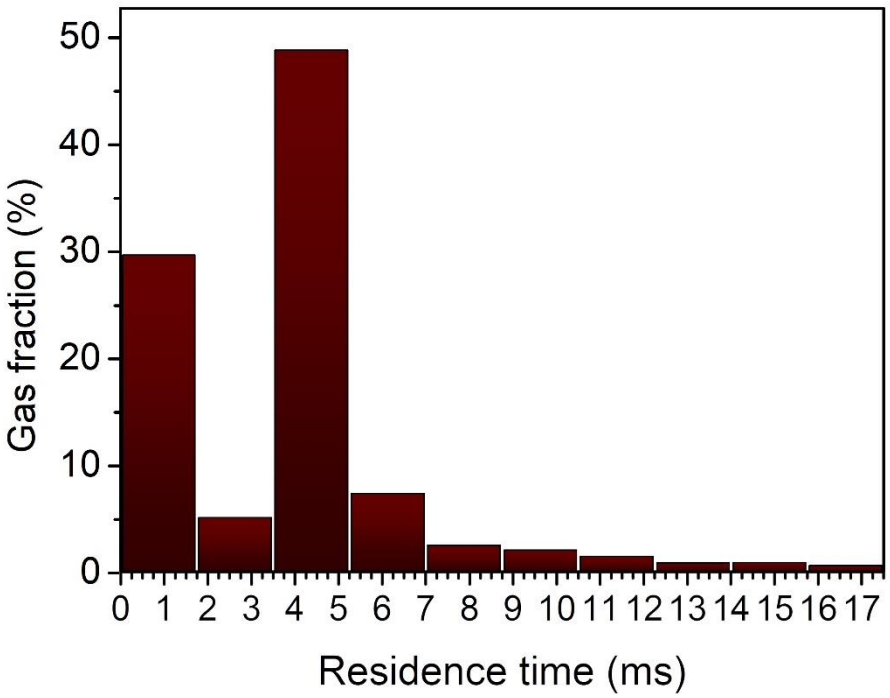

Figure 6: Distribution of gas molecules according to the their residence time between cathode and anode.

Using the calculated trajectories of the gas molecules, obtained from the particle tracing simulations, we can assign residence times to the actual pathways in the reactor. The model reveals that these pathways can be divided into three different zones, see figure 7a. Gas flowing close to the walls (blue region), which displays a high flow velocity in figure 3, has a short residence time (i.e. up to 1.75 ms) between the electrodes in the reactor. Gas in the centre of the reactor (yellow region) which displays a low flow velocity in figure 3, has a longer residence time (i.e. up to 3.5 ms) in the reactor. Gas flowing in between these two regions (orange region) has the longest residence time (i.e. even up to 17.5 ms), due to the presence of a recirculation zone in this area (red region in figure 7a). This recirculation zone is also visualised in figure 7b, displaying the velocity field vectors of the gas flow in the reactor. As shown by the flow vectors highlighted in orange, gas molecules can recirculate in this region, forming a recirculation zone and extending the residence time in the plasma arc. Our model thus reveals a major advantage of the current reactor design, as its geometry favours the formation of a local

recirculation zone near the plasma arc that greatly increases the residence time of the gas in the plasma.

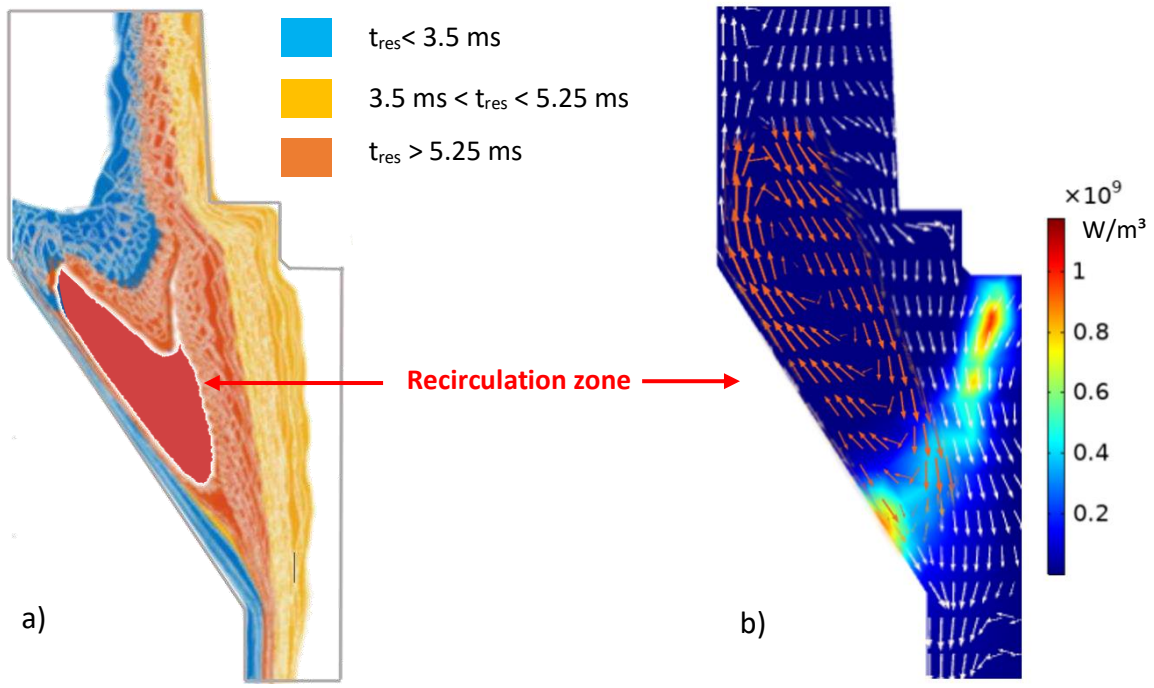

Figure 7: Cross section of the RGA, indicating (a) the molecule trajectories, for which the gas has a residence time lower than 3.5 ms, between 3.5 and 5.25 ms and higher than 5.25 ms when passing between the electrodes, as calculated by the particle tracing simulations. The recirculation zone is highlighted in red. (b) Velocity field vectors of the gas flow in the reactor. The shape of the arc is displayed through a power density profile (see colour scale at the right). The recirculation zone is highlighted with orange arrows.

As molecules flow through the rotating plasma arc, they feel a certain temperature and power density. As shown by the velocity field vectors in the arc in figure 7b, this power density will be significantly higher if they follow the velocity vectors close to the cathode pin or the anode wall where the power density is maximal (cf. the red power density hot-spots in the power density profile). Just like the residence time, the temperature and power density the molecules experience thus strongly depends on the location of the molecule trajectories. Therefore, a similar distribution as for the residence time can be made for the gas temperature that the molecules experience as they flow through the reactor.

This distribution is illustrated in figure 8, displaying the calculated gas temperature experienced by the gas molecules while flowing through the reactor. The temperature intervals of the distribution are chosen to be smaller in the range between 2000 K and 3200 K where the gas conversion is mostly

sensitive to the temperature. This distribution shows that 15% of the gas flows through the reactor where the temperature is below 2000 K, thus not passing the rotating arc a single time when flowing towards the outlet. Note, however, that this fraction is significantly less than in other GA designs, such as a classical (2D) GA or the GA Plasmatron, where 85% of the gas flows through the reactor without actually passing the plasma.[22,27] The largest fraction of the gas (60%) experiences temperatures between 2600 K and 2800 K, which are found in the hot centre of the arc. A small portion of the gas (5%) experience temperatures above 3000 K, which are located near the electrodes of the reactor (power density hot-spots; see figure 7b).

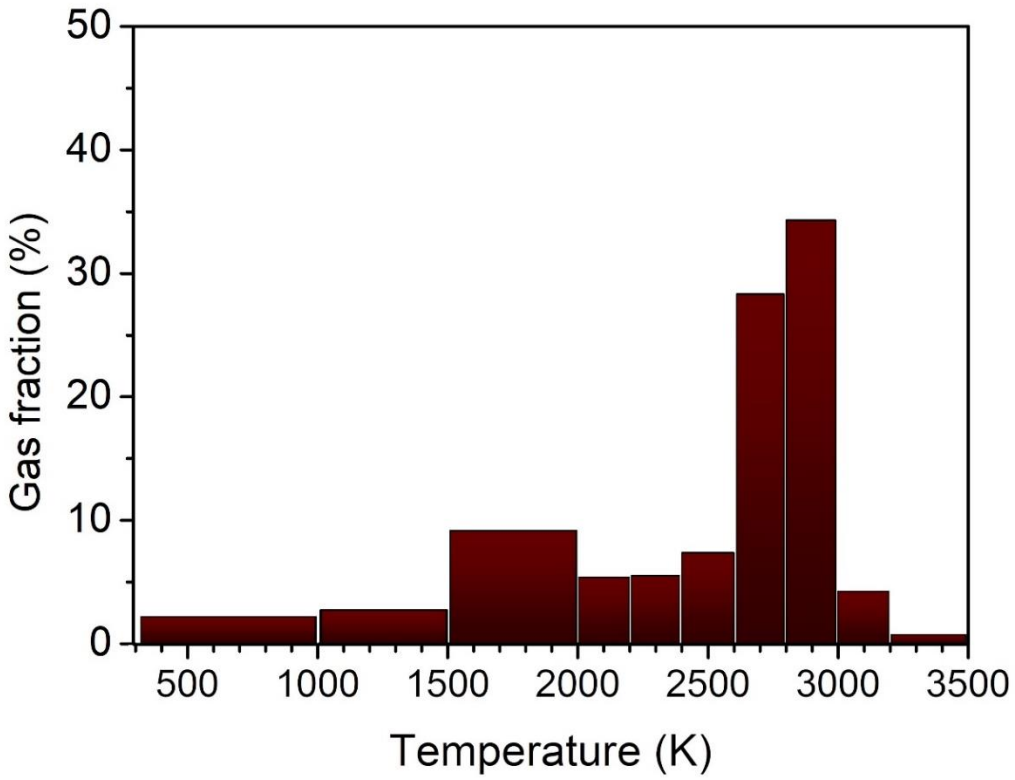

Figure 8: Distribution of gas molecules according to the temperature they experience when flowing through the reactor.

The difference in temperature experienced by the gas molecules, as shown in figure 8, will have its implications for the NO_x formation in each part of the reactor, which will be discussed in the next section.

3.3 NO_x formation in the RGA reactor

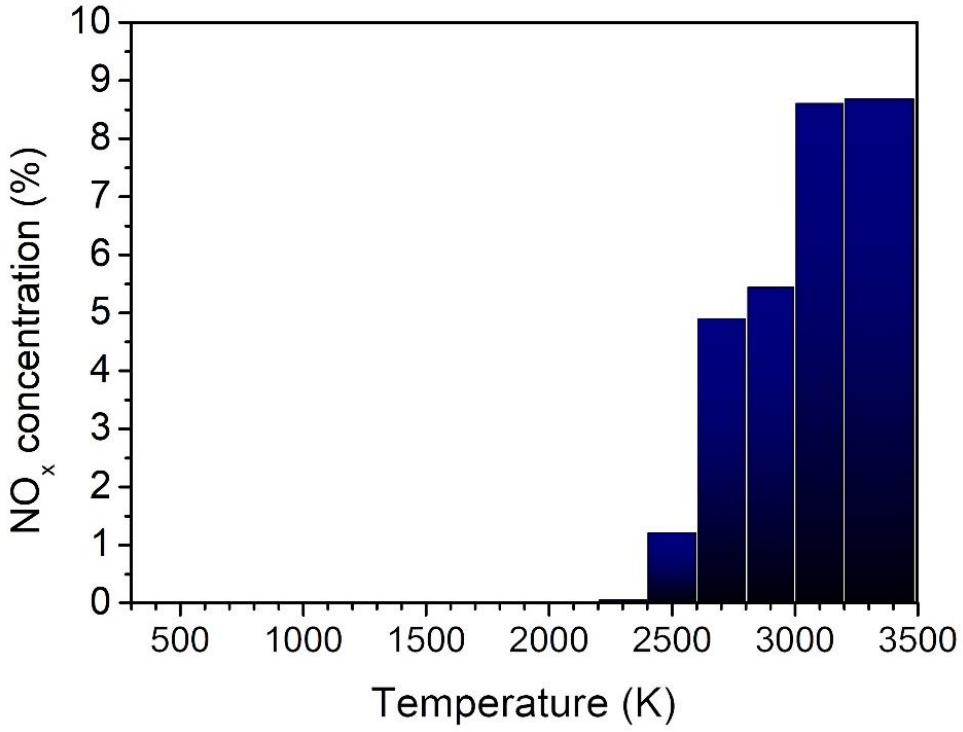

Figure 9: Calculated molar NO_x concentration obtained for each group of gas molecules, experiencing a different temperature, for a gas mixture of 50% N_2 and 50% O_2.

As the gas flows through the reactor, the N_2 and O_2 gas molecules will gradually be converted into NO_x (i.e., NO and NO_2). To calculate the NO_x formation in the RGA, we simulate the plasma chemistry along the trajectories of the gas molecules using the quasi-1D model. The simulation results are presented here for a 50/50 N_2/O_2 mixture, using the gas temperature and power density experienced by the molecules, as calculated by the (corrected) 3D thermal arc model. The peak temperature and power density values in the plasma are presented in the ESI (section S8) for each temperature interval.

The NO_x formation is calculated for each temperature interval in the temperature distribution of figure 8 and is plotted in figure 9. The overall molar NO_x concentration equals 4.29 %, and is calculated by the weighted average over these ten groups, in which the weight is determined by the distribution of the gas presented in figure 8. The figure displays the trend that a higher temperature leads to a higher NO_x concentration, as the higher temperature significantly increases the rate of the plasma reactions to produce more reactive species and thus enhances the plasma-based NO_x formation. The increase in

NOx concentration seems to be the most significant between 2400 K and 3000 K. Below 2400 K, the plasma kinetics are too slow to produce significant amounts of NOx at the given residence times. Above 3000 K, the higher temperature still increases the NO_x formation, but the increase is less significant. At these temperatures both the NO_x formation and destruction reactions are accelerated to a point where equilibrium is reached, approaching an upper limit in the NO_x formation.

The fact that the highest NO_x production is achieved above 2600 K, i.e. in the hot centre of the arc or in the power density hotspots near the electrodes, is important information to consider in reactor design improvement. For our reactor design, this is found beneficial, as figure 6 indicated that more than 65% of the gas experiences temperatures between 2600 K and 3500 K. This fraction is thus responsible for most of the NO_x production (i.e. 98% of the NO_x produced in the reactor), indicating that, in these conditions, our model could be narrowed down to simulating only this fraction of the gas.

Furthermore, these results also indicate that the NO_x production in our RGA would greatly improve if a higher fraction of the gas would experience these high temperatures. Possible reactor design optimization of our RGA reactor should thus aim to increase the fraction of gas flowing through the centre of the arc (i.e. the 2600-3000 K intervals in figure 8 and 9) or near the surface of the electrodes (i.e. the 3000-3500 K intervals in figure 8 and 9). The first condition could be achieved by reducing the size of the cone-shaped anode of the reactor, so the arc would, once formed in the cone shape, rotate inside the outlet instead of the cone. Since this would fill the outlet with high temperature plasma, gas molecules would be forced to flow through these high temperature zones, increasing the overall NO_x production. The second condition could be achieved by reducing the distance between the anode wall and the cathode pin. While the flow dynamics would need to be revaluated for this change, it is to be expected that the hotspots near the electrode surfaces would become proportionally more important as the surfaces get closer together, resulting in a higher fraction of gas flowing through these hotspots.

3.4 Underlying chemistry for NO_x production, and the role of vibrational excitation

The quasi-1D model also reveals the underlying plasma chemistry of NO_x production, providing deeper insight into why certain plasma conditions lead to a higher or lower NO_x concentration, which is very valuable information for further reactor development. As reported by Wang et al.[22] and Vervloessem et al.[27], the plasma chemistry in GA reactors is defined by the vibrational excitation of N_2 and O_2 molecules by the high energy electrons in the plasma. Indeed, the electron temperature in GA plasmas is typically around 1 eV (11 605 K), at which vibrational excitation the most favoured excitation pathway.[22,27] Hence, GA plasmas are often characterized by a vibrational temperature that is higher than the translational temperature (i.e. the gas temperature).

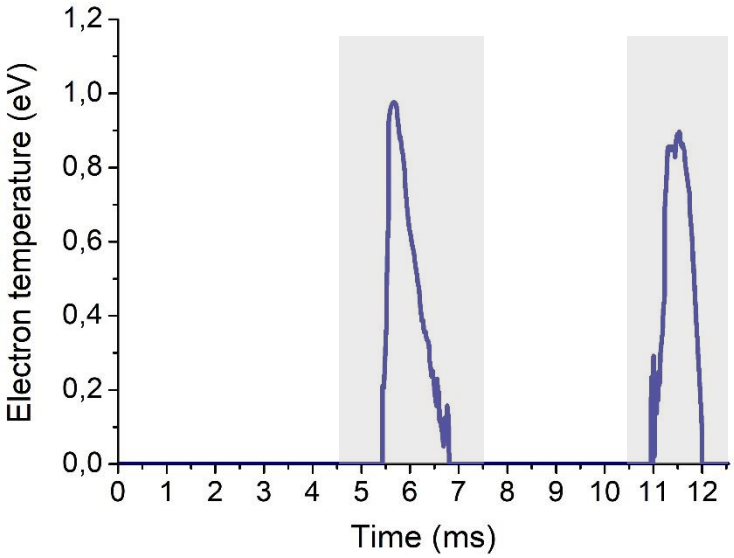

Figure 10: Time evolution of the calculated electron temperature felt by molecules flowing close to the centre of the arc. The grey zones indicate when the molecules pass through the rotating arc.

Figure 10 displays the electron temperature calculated by the quasi-1D model felt by molecules flowing close to the centre of the RGA reactor and experiencing two arc rotations. It is clear that the electron temperature in the arc indeed lies around 1 eV, and therefore a significant fraction of the electron energy is transferred to vibrational excitation of the gas. This is especially important for N_2, since vibrational excitation of N_2 facilitates the splitting of the strong triple bond of the molecule (≈ 10 eV) and promotes NO_x production through the Zeldovich mechanism:

$O + N_2(V) \rightarrow N + NO$

$N + O_2(V) \rightarrow O + NO$

However, at high gas temperature around 3000 K, which is a typical value for a GA at atmospheric pressure[15,27,44] (cf. also figure 5 and 8 above), the lifetime of these vibrationally excited molecules ($N_2(V)$ and $O_2(V)$) is limited, because a high gas temperature greatly increases the rate of vibrational-translational (VT) relaxation collisions, in which the vibrational energy from an excited molecules is lost to gas heating. Thus, a thermal equilibrium between the translational and vibrational temperature is eventually achieved.

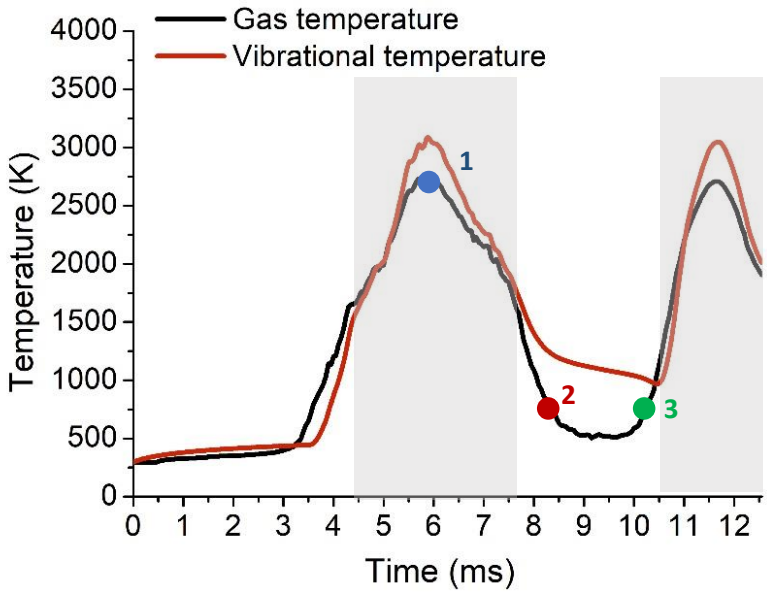

Figure 11: Time evolution of the calculated gas and vibrational temperature of molecules flowing close to the centre of the arc. The grey zones indicate when the molecules pass through the rotating arc. The coloured numbers (1, 2, 3) indicate the time points at which the VDF's are plotted in figure 13.

In the RGA, however, the gas cools down very fast after leaving the arc (cf. figure 5), i.e., after every arc rotation, inhibiting the VT relaxation and allowing for vibrationally excited molecules to exist for a significantly longer time. Figure 11 depicts the time evolution of the gas and vibrational temperature for a molecule trajectory near the centre of the reactor, experiencing two arc rotations. The fast cooling in between the arc rotations develops a clear non-equilibrium between both temperatures. The characteristic timescale of VT relaxation is plotted in figure 12, showing that the fast cooling drastically slows down the vibrational relaxation. Indeed, while VT relaxation operates on a sub-ms

timescale in the arc (see figure 12), it only occurs on a seconds timescale outside the hot plasma zone, so the lifetime of the vibrationally excited molecules is on the order of seconds, once they are created in the arc.

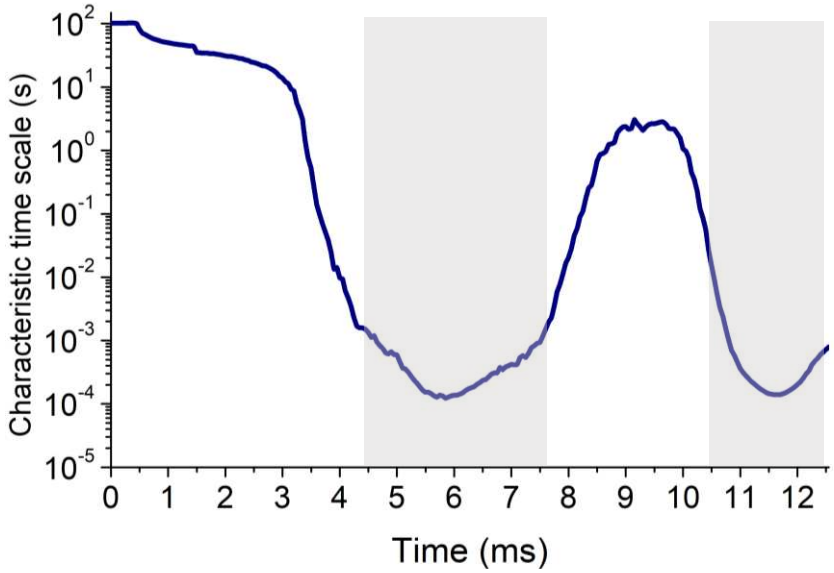

Figure 12: Time evolution of the characteristic timescale of VT relaxation for molecules flowing close to the centre of the arc. The grey zones indicate when the molecules pass through the rotating arc.

The extended lifetime of the vibrationally excited molecules after leaving the arc, and the presence of vibrational-translational (VT) equilibrium inside the arc are also noticeable from the calculated vibrational distribution function (VDF) of N_2, plotted in figure 13. While the vibrational temperature only accounts for the excitation of the first vibrational level of the N_2 stretching mode, the VDF indicates how the energy is distributed among all vibrational levels of N_2 by presenting the relative population of each vibrational level. Figure 13 illustrates the VDF's of N_2 at three different time points of the temperature profile in figure 11, displaying the evolution of the VDF during the fast cooling. As a reference, the Boltzmann distribution functions at the corresponding calculated gas temperatures are also plotted with dashed lines in the same colour, to indicate the degree of vibrational-translational (VT) (non)equilibrium. The VDF's all exhibit a Boltzmann distribution, but only inside the arc (point 1), the VDF coincides more or less with the Boltzmann distribution defined by the gas temperature, showing that the gas is in VT equilibrium due to the high temperature in the arc. Once the cooling starts and VT-relaxation processes are inhibited, the vibrational levels of N_2 stay

highly populated. They still exhibit a Boltzmann distribution, but with a clear overpopulation compared to the Boltzmann distribution at the corresponding gas temperature (points 2 and 3). Even 1 ms after the arc rotation (cf. time point 3 in figure 11), these higher vibrational levels are still strongly overpopulated.

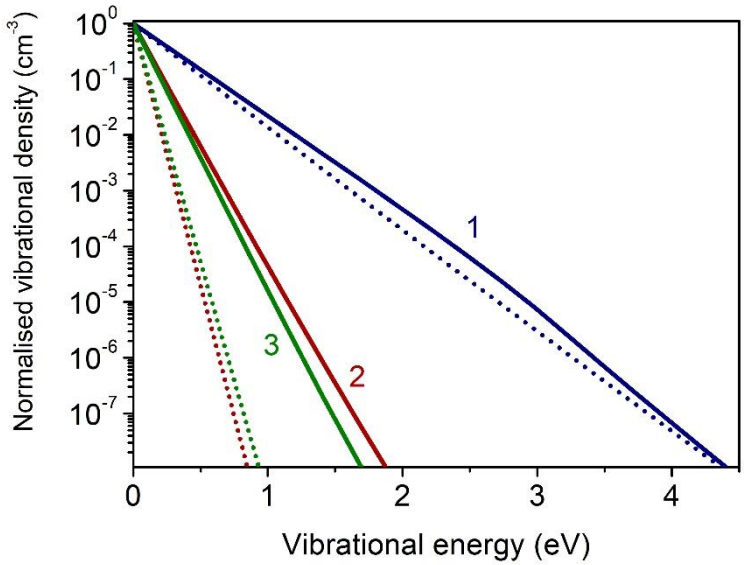

Figure 13: VDFs at three different points in time indicated in the temperature profile in figure 11. The full line represent the calculated VDFs, while the dotted lines represent the Boltzmann distributions at the corresponding gas temperature.

Thus, as the vibrational levels are highly populated even when no plasma is present, vibrational splitting of N_2 and the vibrationally-promoted Zeldovich reactions still occur outside of the arc. Our model predicts that more than 99 % of the NO_x formation proceeds through the vibrationally-promoted Zeldovich mechanism in the RGA. This uninterrupted NO_x production is illustrated in figure 14, showing the calculated NO_x production rate as a function of time, for gas molecules flowing close to the centre of the reactor, hence experiencing two full arc rotations. The NO_x formation clearly rises when the molecules encounter the arc, but even in between two arc rotations, the NO_x formation is still significant, also because the lower temperature inhibits back-reactions that destroy NO_x. Although the NO_x production in between two arc rotation certainly is beneficial for the performance of the RGA, figure 14 indicates that the great majority of the NO_x production occurs inside the (second) arc, due to the high electron density and the formation of many reactive plasma species.

The model thus suggests that higher NO_x production would be achieved if the residence time in the arc during each rotation would be longer. Possible design modifications that would either slow down the rotational movement of the arc or locally increase the residence time of the gas in the hot plasma zone are thus important targets for design improvements of this RGA reactor.

3.5 Comparison to experimental results

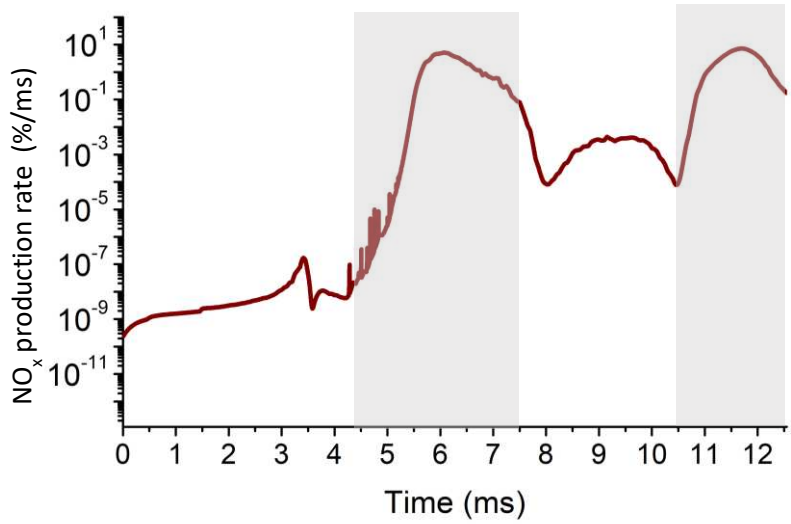

Figure 14: Time evolution of the molar NO_x production rate for molecules flowing close to the centre of the arc. The grey zones indicate when the molecules pass through the rotating arc.

To test the predictive capabilities of our model, we compare in figure 15 the calculated NO_x concentrations and energy cost with experimental data obtained in the RGA reactor, at the same applied power of 106 W and flow rate of 2 L min^{-1} , and for N_2-O_2 gas ratios varying from 20-80 % to 80-20 %.[45] Details about the experimental setup are presented in the ESI (section S8). For each gas feed ratio, the NO_x concentration is calculated for the ten groups in the molecule distribution displayed in figure 6. Subsequently, the overall NO_x concentration is calculated by weighted average over the ten groups. We evaluate the total NOx concentration and not the separate NO and NO_2 concentrations, as these two compounds are easily converted into each other. Even in the tubing to the detector device,

NO can oxidize to NO_2, changing the ratio of the output gas. For this reason, the calculated NO/NO_2 ratio is considerably higher than the experimental one. Indeed, the calculated NO/NO_2 ratio lies around 3.9 (calculated at the outlet of the reactor), while the experimental NO/NO_2 ratio lies around 0.44, but it is measured after flowing through the tubing of the detection device, hence this comparison is not meaningful. Both our modelling and experimental results indicate that the produced amounts of N_2O are very low (below 0.01 %), which is beneficial given its danger as greenhouse gas. The modelling results are in good agreement with the experiments, both in absolute values and in showing a very similar trend as a function of the gas feed ratio. "The maximum NOx concentration of 3.35 %, and lowest energy cost of 2.4 MJ/mol, is provided by the 40-60 % N2-O2 mixture, where both N2 and O2 are present in high amounts to form NOx. In this mixture 3.84 % of the applied energy is eventually stored in the produced NOx molecules, whereas the rest is used to heat or ionize, excite or dissociate the gas molecules but without NOx formation. For this reason, the achieved energy cost of 2.4 MJ/mol is still significantly higher than the energy cost of the Haber-Bosch process (0.48 MJ/mol). Nevertheless, it is already better than obtained in other atmospheric pressure plasma reactor types. Furthermore, as discussed in section 3.3, our modelling approach allows us to propose several design optimizations to further improve the performance of the process."

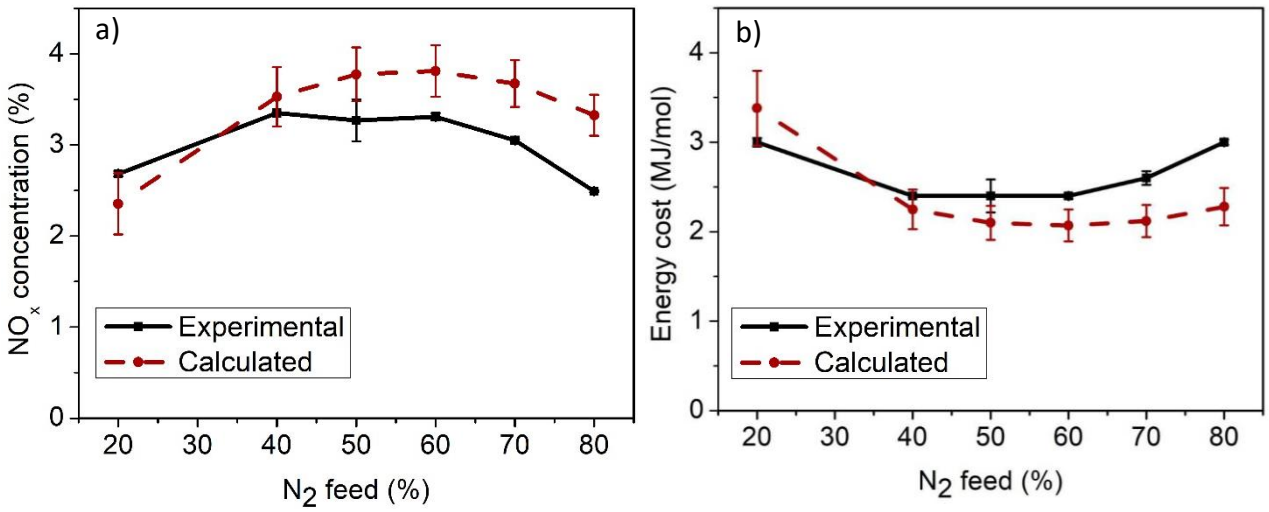

Figure 15: Calculated and experimental a) molar NO_x concentrations and b) energy cost at different N_2 feed ratios, at an applied power of 106 W and flow rate of 2 L min^{-1}. The error bars of the experimental values are obtained from the standard deviation of the measurements, but they are sometimes too small to be visible. The error bars of the calculated values are based on the sensitivity of the quasi 1D-model to the standard deviation of the average peak temperature in the plasma, as shown in the supporting information (section S8).

4 Conclusion

Computational models can be valuable in the search for optimal reactor configurations for plasma-based sustainable chemistry applications, as they can save time and money in the optimisation process. We present here a combined modelling approach for describing the fluid dynamics, the plasma behaviour and the plasma chemistry in a GA reactor in five complementary models. Using this method we present a very comprehensive description of plasma-based NO_x formation in a RGA reactor.

The model reveals that the characteristic vortex flow formed by the tangential flow inlet drags the arc around in a rotational movement. Due to the great difference in flow velocity within the vortex flow and the formation of a recirculation zone near the arc, the gas can experience a residence time between 0 and 17.5 ms, depending on its flow trajectory in the reactor. The model shows that 19% of the gas flows through the reactor without being converted by the plasma, while 65% of the gas experiences two arc rotations. 98% of the NO_x formation occurs within this 65%, as this gas fraction flows through a hot spot in the plasma near the cathode pin. The model also reveals the underlying plasma chemistry, demonstrating the importance of the vibrationally-promoted NO_x formation through the Zeldovich mechanism. Due to the fast cooling of the gas, each time after the arc rotation, VT relaxation is inhibited, strongly increasing the lifetime of vibrationally excited molecules. Furthermore, these lower temperatures inhibit NO_x destroying back-reactions. As the vibrational energy levels of N_2 remain significantly excited between the arc rotations, N_2 splitting and NO_x formation are shown to continue in between two arc rotations, albeit at a lower rate. Good agreement with experimental data at different gas ratios demonstrates that our modelling approach can provide a realistic picture of the flow and plasma behaviour in the RGA reactor. This approach can also be used

for modelling reactor design improvements for other gas conversion applications, when the plasma chemistry is available.

5.Conflicts of Interests

There are no conflicts of interests to declare.

6. Acknowledgments

This research was supported by the Excellence of Science FWO-FNRS project (FWO grant ID GoF9618n, EOS ID 30505023), the European Research Council (ERC) under the European Union's Horizon 2020 research and innovation programme (grant agreement No 810182 – SCOPE ERC Synergy project), the Flemish Government through the Moonshot cSBO project D2M (HBC.2019.0107) and through long-term structural funding (Methusalem). The calculations were performed using the Turing HPC infrastructure at the CalcUA core facility of the Universiteit Antwerpen (UAntwerpen), a division of the Flemish Supercomputer Center VSC, funded by the Hercules Foundation, the Flemish Government (department EWI) and the UAntwerpen. We also thank J.-L. Liu for building the RGA reactor.

References

(1) R. K. Pachauri and L. A. Meyer. *Climate Change 2014: Synthesis Report. Contribution of Working Groups I, II and III to the Fifth Assessment Report of the Intergovernmental Panel on Climate Change, Geneva, Switzerland, 2014*; 2014.

(2) Bogaerts, A.; Neyts, E. C. Plasma Technology: An Emerging Technology for Energy Storage. *ACS Energy Lett.* **2018**, *3*, 1013–1027.

(3) Snoeckx, R.; Bogaerts, A. Plasma Technology – a Novel Solution for CO_2 Conversion? *Chem. Soc. Rev.* **2017**, *46*, 5805–5863.

(4) Fridman, A. *Plasma Chemistry*; Cambridge University Press: Cambridge, U.K., 2008.

(5) Patil, B. S.; Wang, Q.; Hessel, V.; Lang, J. Plasma N2-Fixation: 1900–2014. *Catal. Today* **2015**, *256*, 49–66.

(6) Asisov, R. I.; Givotov, V. K.; Rusanov, V. D.; Fridman, A. High Energy Chemistry (Khimia Vysokikh Energij). *Sov. Phys.,* **1980**, *14*, 366.

(7) Britun, N.; Silva, T.; Chen, G.; Godfroid, T.; Van Der Mullen, J.; Snyders, R. Plasma-Assisted CO2 Conversion: Optimizing Performance via Microwave Power Modulation. *J. Phys. D. Appl. Phys.* **2018**, *51*.

(8) Van Alphen, S.; Vermeiren, V.; Butterworth, T.; Van Den Bekerom, D. C. M.; Van Rooij, G. J.; Bogaerts, A. Power Pulsing to Maximize Vibrational Excitation Efficiency in N2 Microwave Plasma: A Combined Experimental and Computational Study. *J. Phys. Chem. C* **2020**, *124*, 1765–1779.

(9) Wolf, A. .; Righart, T. W.; Peeters, F. J.; Bongers, W. .; van de Sanden, M. C. Implications of Thermo-Chemical Instability on the Contracted Modes in CO2 Microwave Plasmas. *Plasma Sources Sci. Technol.* **2020**, *29*, 025005.

(10) van den Bekerom, D. C. M.; Palomares Linares, J. M.; Verreycken, T.; van Veldhuizen, E. M.; Nijdam, S.; Bongers, W.; Van de Sanden, R.; Van Rooij, G. J. The Importance of Thermal Dissociation in CO2 Microwave Discharges Investigated by Power Pulsing and Rotational Raman Scattering. *Plasma Sources Sci. Technol.* **2019**.

(11) Patil, B. S.; van Rooij, G. J.; Peeters, F. J. J.; Medrano, J. A.; Gallucci, F.; Lang, J.; Wang, Q.; Hessel, V. Plasma Assisted Nitrogen Oxide Production from Air: Using Pulsed Powered Gliding Arc Reactor for a Containerized Plant. *AIChE J.* **2017**, *64*, 526–537.

(12) Fridman, A.; Gutsol, A.; Gangoli, S. Characteristics of Gliding Arc and Its Application in Combustion Enhancement. *J. Prop. Power* **2008**, *24*, 1216–1228.

(13) Indarto, A.; Yang, D.; Choi, J.; Lee, H.; Song, H. Gliding Arc Plasma Processing of CO2 Conversion. *J. Hazard. Mat.* **2005**, *76*, 025110.

(14) Ramakers, M.; Trenchev, G.; Heijkers, S.; Wang, W.; Bogaerts, A. Gliding Arc Plasmatron: Providing an Alternative Method for Carbon Dioxide Conversion. *ChemSusChem* **2017**, *10*, 2642–2652.

(15) Slaets, J.; Aghaei, M.; Ceulemans, S.; Van Alphen, S.; Bogaerts, A. CO2 and CH4 Conversion in "Real" Gas Mixtures in a Gliding Arc Plasmatron: How Do N2 and O2 Affect the Performance? *Green Chem.* **2020**, *22*, 1366–1377.

(16) Cleiren, E.; Heijkers, S.; Ramakers, M.; Bogaerts, A. Dry Reforming of Methane in a Gliding Arc Plasmatron: Towards a Better Understanding of the Plasma Chemistry. *ChemSusChem* **2017**, *10*, 3864–3864.

(17) Van Laer, K.; Bogaerts, A. Improving the Conversion and Energy Efficiency of Carbon Dioxide Splitting in a Zirconia-Packed Dielectric Barrier Discharge Reactor. *Energy Technol.* **2015**, *3*, 1038–1044.

(18) Michielsen, I.; Uytdenhouwen, Y.; Pype, J.; Michielsen, B.; Mertens, J.; Reniers, F.; Meynen, V.;

Bogaerts, A. CO2dissociation in a Packed Bed DBD Reactor: First Steps towards a Better Understanding of Plasma Catalysis. *Chem. Eng. J.* **2017**, *326*, 477–488.

(19) Mizushima, T.; Matsumoto, K.; Sugoh, J. I.; Ohkita, H.; Kakuta, N. Tubular Membrane-like Catalyst for Reactor with Dielectric-Barrier- Discharge Plasma and Its Performance in Ammonia Synthesis. *Appl. Catal. A Gen.* **2004**, *265*, 53–59.

(20) Mindi Bai; Wang Ning; Zhitao Zhang; Mindong Bai; Xiyao Bai. Plasma Synthesis of Ammonia with a Microgap Dielectric Barrier Discharge at Ambient Pressure. *IEEE Trans. Plasma Sci.* **2004**, *31*, 1285–1291.

(21) Uytdenhouwen, Y.; Alphen, S. Van; Michielsen, I.; Meynen, V.; Cool, P.; Bogaerts, A. A Packed-Bed DBD Micro Plasma Reactor for CO 2 Splitting : Does Size Matter ? *Chem. Eng. J.* **2018**, *348*, 557–568.

(22) Wang, W.; Patil, B.; Heijkers, S.; Hessel, V.; Bogaerts, A. Nitrogen Fixation by Gliding Arc Plasma: Better Insight by Chemical Kinetics Modelling. *ChemSusChem* **2017**, *10*, 2110.

(23) Indarto, A.; Choi, J.-W.; Lee, H.; Song, H. K. Conversion of CO2 by Gliding Arc Plasma. *Env. Eng.* **2006**, *23*, 1033–1043.

(24) Kalra, C.; Cho, Y.; Gutsol, A.; Fridman, A. Gliding Arc in Tornado Using a Reverse Vortex Flow. *Rev. Sc. Instrum.* **2005**, *76*, 025110.

(25) Liu, J.; Park, H.; Chung, W.; Park, D. High-Efficient Conversion of CO2 in AC-Pulsed Tornado Gliding Arc Plasma. *Plasma Chem. Plasma Process.* **2015**, *09*.

(26) Nunnaly, T.; Gutsol, K.; Rabinovich, A.; Fridman, A.; Gutsol, A.; Kemoun, A. A Gutsol, A Kemoun, Dissoaciation of CO2 in a Low Current Gliding Arc Plasmatron. *J. Phys. D Appl. Phys* **2011**, *44*, 274009.

(27) Vervloessem, E.; Aghaei, M.; Jardali, F.; Hafezkhiabani, N.; Bogaerts, A. Plasma-Based N 2

Fixation into NO X : Insights from Modeling toward Optimum Yields and Energy Costs in a Gliding Arc Plasmatron. *ACS Sustain. Chem. Eng.* **2020**, *8*, 9711–9720.

(28) Puliyalil, H.; Lašič Jurković, D.; Dasireddy, V. D. B. C.; Likozar, B. A Review of Plasma-Assisted Catalytic Conversion of Gaseous Carbon Dioxide and Methane into Value-Added Platform Chemicals and Fuels. *RSC Adv.* **2018**, *8*, 27481–27508.

(29) Lašič Jurković, D.; Liu, J. L.; Pohar, A.; Likozar, B. Methane Dry Reforming over Ni/Al2O3 Catalyst in Spark Plasma Reactor: Linking Computational Fluid Dynamics (CFD) with Reaction Kinetic Modelling. *Catal. Today* **2020**, *362*, 11–21.

(30) Liu, J. L.; Wang, X.; Li, X. S.; Likozar, B.; Zhu, A. M. CO2 Conversion, Utilisation and Valorisation in Gliding Arc Plasma Reactors. *J. Phys. D. Appl. Phys.* **2020**, *53*.

(31) Trenchev, G.; Kolev, S.; Bogaerts, A. A 3D Model of a Reverse Vortex Flow Gliding Arc Reactor. *Plasma Sources Sci. Technol.* **2016**, *25*.

(32) Kolev, S.; Sun, S.; Trenchev, G.; Wang, W.; Wang, H.; Bogaerts, A. Quasi-Neutral Modeling of Gliding Arc Plasmas. *Plasma Process. Polym.* **2017**, *14*, 8–11.

(33) Kolev, S.; Bogaerts, A. 2D Model for a Gliding Arc Discharge. *Plasma Sources Sci.* **2015**, *24*, 015025.

(34) Sun, S. R.; Kolev, S.; Wang, H. X.; Bogaerts, A. Coupled Gas Flow-Plasma Model for a Gliding Arc: Investigations of the Back-Breakdown Phenomenon and Its Effect on the Gliding Arc Characteristics. *plasma sources sci. Technol.* **2017**, *26*, 015003.

(35) Sun, S. R.; Kolev, S.; Wang, H. X.; Bogaerts, A. Investigations of Discharge and Post-Discharge in a Gliding Arc: A 3D Computational Study. *plasma sources sci. Technol.* **2017**, *26*, 055017.

(36) Ingels, R.; Graves, D. B. Improving the Efficiency of Organic Fertilizer and Nitrogen Use via Air Plasma and Distributed Renewable Energy. *Plasma Med.* **2015**, *5*, 257–270.

(37) Menter, F. R.; Kuntz, M.; Langtry, R. Ten Years of Industrial Experience with the SST Turbulence Model. *Turbul. Heat Mass Transf.* **2003**, *4*, 625–632.

(38) COMSOL Multiphysics® v. 5.5. Www.Comsol.Com. COMSOL AB, Stockholm, Sweden.

(39) Trenchev, G.; Nikiforov, A.; Wang, W.; Kolev, S.; Bogaerts, A. Atmospheric Pressure Glow Discharge for CO2 Conversion: Model-Based Exploration of the Optimum Reactor Configuration. *Chem. Eng. J.* **2019**, *362*, 830–841.

(40) Trenchev, G.; Bogaerts, A. Dual-Vortex Plasmatron – A Novel Plasma Source for CO2 Conversion. *J. CO2 Util.* **2020**, *39*, 101152.

(41) Pancheshnyi, S.; Eismann, B.; Hagelaar, G. J. M.; Pitchford, L. C. Computer code ZDPlasKin, http://www.zdplaskin.laplace.univ-tlse.fr (University of Toulouse, LAPLACE, CNRS-UPSINP, Toulouse, France, 2008).

(42) Hagelaar, G. J. M.; Pitchford, L. C. Solving the Boltzmann Equation to Obtain Electron Transport Coefficients and Rate Coefficients for Fluid Models. *Plasma Sources Sci. Technol.* **2005**, *14*, 722–733.

(43) Alves, L. L.; Bogaerts, A.; Guerra, V.; Turner, M. M. Foundations of Modelling of Nonequilibrium Low-Temperature Plasmas. *Plasma Sources Sci. Technol.* **2018**, *27*.

(44) Trenchev, G.; Kolev, S.; Wang, W.; Ramakers, M.; Bogaerts, A. CO2 Conversion in a Gliding Arc Plasmatron: Multidimensional Modeling for Improved Efficiency. *J. Phys. Chem. C* **2017**, *121*, 24470–24479.

(45) Jardali, F.; Van Alphen, S.; Creel, J.; Ahmadi Eshtehardi, Hamid Axelsson, M.; Ingels, R.; Snyders, R.; Bogaerts, A. NOx Production in a Rotating Gliding Arc Plasma: Potential Avenue for Sustainable Nitrogen Fixation. *Green Chem.* **2021**, Accepted for publication.